Molecular dynamics — potential of mean force calculations as a tool for understanding ion permeation and selectivity in narrow channels

Toby W. Allen [a],*, Olaf S. Andersen [b], Benoit Roux [b],[1]

[a] *Department of Chemistry, University of California, Davis, One Shields Avenue, Davis CA 95616, USA*
[b] *Department of Physiology and Biophysics, Weill Medical College of Cornell University, USA*

Abstract

Ion channels catalyze the permeation of charged molecules across cell membranes and are essential for many vital physiological functions, including nerve and muscle activity. To understand better the mechanisms underlying ion conduction and valence selectivity of narrow ion channels, we have employed free energy techniques to calculate the potential of mean force (PMF) for ion movement through the prototypical gramicidin A channel. Employing modern all-atom molecular dynamics (MD) force fields with umbrella sampling methods that incorporate one hundred 1–2 ns trajectories, we find that it is possible to achieve semi-quantitative agreement with experimental binding and conductance measurements. We also examine the sensitivity of the MD-PMF results to the choice of MD force field and compare PMFs for potassium, calcium and chloride ions to explore the basis for the valence selectivity of this narrow and uncharged ion channel. A large central barrier is observed for both anions and divalent ions, consistent with lack of experimental conductance. Neither anion or divalent cation is seen to be stabilized inside the channel relative to the bulk electrolyte and each leads to large disruptions to the protein and membrane structure when held deep inside the channel. Weak binding of calcium ions outside the channel corresponds to a free energy well that is too shallow to demonstrate channel blocking. Our findings emphasize the success of the MD-PMF approach and the sensitivity of ion energetics to the choice of biomolecular force field.
© 2006 Elsevier B.V. All rights reserved.

Keywords: Ion channel; Ion permeation; Ion selectivity; Potential of mean force; Free energy; Molecular dynamics; Gramicidin

1. Introduction

Bilayer spanning channels are integral membrane proteins that catalyze the passage of charged and polar molecules across cell membranes. Ion movement through ion channels is an electrodiffusive process, in which many channels can distinguish among different ions based on valence and size (Hille, 2001). Since the pioneering studies of Hodgkin and Huxley [1,2], over five decades of structural and functional studies have sought to understand the mechanisms of permeation and ion selectivity in ion channels. Recent advances in the structure determination of ion channel proteins [3–8] provide the structural underpinnings for detailed mechanistic studies of ion permeation. But it remains a significant challenge to relate the molecular anatomy to the molecular physiology. To fully understand the mechanisms of ion permeation and selectivity, one needs to understand the energetics of ion-channel interactions, which underlies both equilibrium ion binding and the kinetics of ion movements.

Computer simulation plays an important role in providing a molecular level understanding of ion transport that maybe difficult to extract from experiment alone due to the wide gap between molecular and observation timescales [9]. Computer simulations also face significant challenges because of the long time scales (ion transit times through the channel) in ion permeation. To overcome this problem, we have developed methodologies that not only can describe the mechanisms of permeation and selectivity of ion channels, but also establish a framework that connects atomic-level simulation and experimental channel measurements.

The gramicidin A (gA) channel is a single stranded, right-handed $\beta^{6.3}$-helical dimer [10], with known structure [11–14]

---

* Corresponding author. Tel.: +1 530 754 5968; fax: +1 530 752 8995.
E-mail address: twallen@ucdavis.edu (T.W. Allen).
[1] Benoit Roux's present address is Institute of Molecular Pediatric Sciences Center for Integrative Science, University of Chicago, Chicago, IL, USA.

and decades of functional studies [15–19] making it an ideal prototype for studies of ion permeation and selectivity in narrow pores. The gA channel poses a significant challenge for computational investigation. Common to all channels, it becomes necessary to describe the process by which ions leave bulk electrolyte to enter a narrow pore. This becomes a challenge because of the need to represent both the interactions between ions and bulk water and ions and the protein backbone (where the ion will be in an almost completely desolvated state). Particular difficulties arise in the case of gA channels because of its single-file pore and its unique orientation of carbonyl groups, almost parallel to the channel axis. That is the peptide backbone in gA channels does not solvate the ion as would a hydration shell or the selectivity filter in potassium channels where carbonyl dipoles take on a more radial orientation [3]. This means that the mechanisms of permeation and selectivity in gA channels are subtle and difficult to characterize, making gA channels suitable to evaluate computational strategies.

Many permeation models have used a single rigid structure and continuum methods to represent interactions within the narrow pore (see Ref. [20] for a critique). A physically correct model of ion channel function, which incorporates the consequences of thermal fluctuations, is important in cases where the ion energetics is very sensitive to the precise location

of protein atoms [20]. Fig. 1A shows the fluctuation of carbonyl groups in gA of up to 0.63 Å. The effects of these fluctuations on the potential energy profile for an ion through a rigid gA model are shown in Fig. 1B, revealing clearly why a dynamical model is needed. In addition, these fluctuations demonstrate the protein's ability to undergo flexible responses to external perturbations, such as the presence of an ion [20] that would be missing in a rigid model. For this reason, molecular dynamics (MD) becomes the method of choice for investigating ion channel function. Fortunately, gA is small enough to allow for thorough configurational sampling with MD simulation and modern computational resources [21,22] such that there no longer is a need to employ unphysical approximations.

The long timescales of ion conduction events, on the order of 10–100 ns, make it difficult to observe and calculate ion currents from unbiased simulation. This difficulty can be overcome by extracting the equilibrium distribution of coordinates governing conduction with the use of MD simulation and free energy calculation techniques and thereby unveil microscopic mechanisms and establish a formalism for making contact with experiment. Configurational sampling of a fully atomistic system consisting of an ion channel protein, electrolyte solutions and a phospholipid bilayer can be used to extract an equilibrium potential of mean force (PMF) that incorporates all of the thermal fluctuations of the system and which describes the governing forces of ion conduction. Phenomenological conduction models, consistent with the PMF calculation can then be utilized to estimate the ion flux through the ion channel, as well as ion binding to the channel. Such calculations also shed light on the mechanisms of permeation because the free energy profiles can be resolved spatially — and as a function of other interesting coordinates such as ion hydration.

Despite the theoretical advantages of this approach, several attempts to capture a PMF for permeation through gA channels [23–25] led to PMFs that predicted ion fluxes that were many orders of magnitude too low to be compatible with experiment. A major reason for the difficulties in predicting ion fluxes can be traced to the relatively short simulation times used in these studies. As computational methods have become more powerful, it has become possible to greatly extend the simulation times and thus obtain thorough equilibrium sampling [26,27]. Further improvements could be achieved by correcting for the artifacts of periodicity and lack of hydrocarbon dielectric response. Taken together, these improvements permitted the prediction of ion binding constants and conductance values that approach semi-quantitative agreement with experimental results. Indeed, this MD-PMF approach can yield results consistent with all available experimental data and describes, at a molecular level, the controlling factors in ion permeation and selectivity in a narrow pore.

The particular charge distribution of the gA channel prohibits a clearly identifiable structure-based interpretation of selectivity mechanisms. Despite the neutrality of gA, the channel is highly selective for monovalent cations and impermeable to anions [17,28]. For example, although K^+ and Cl^- have similar hydration free energies [29], K^+ permeates relatively easily, whereas Cl^- cannot be detected to go through the channel. Part of
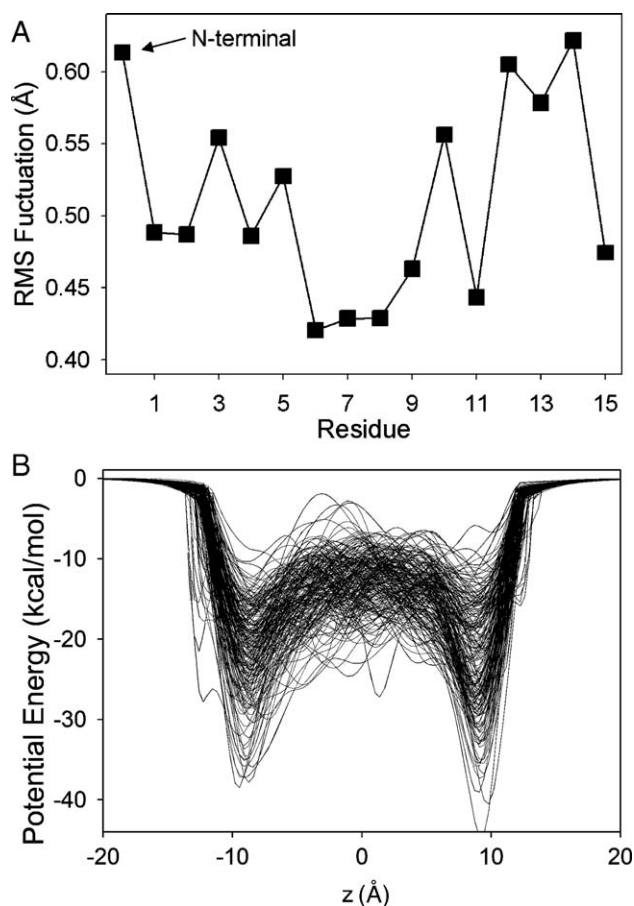

Fig. 1. (A) RMS fluctuations in residues of the gA channel during 4 ns of MD simulation (residue 0 corresponds to the formyl carbonyl oxygen at the formyl-NH$_2$ terminus). (B) Potential profiles from solution to Poisson's equation (expressed as potential energy) for 194 samples from MD.

the answer is likely to be the poor solvation of anions by peptide backbone-mimicking solvents [17]. In addition, the asymmetry in the charge distribution of the β-helix may be important [10,30]. In 1981, Urry suggested that the ability of gA to bind cations was due to the ability of the outer carbonyls (which in a right-handed helix are the Leu10–Trp11, Leu12–Trp13 and Leu14–Trp15 carbonyl groups), which are not tied up in H-bonds within the β-helix, to deflect and stabilize the cation [30]. Conversely, Sung and Jordan proposed that these outwardly directed carbonyls would present a barrier to an approaching negative ion, further postulating that once the anion enters the channel it would be stabilized relative to the bulk [31] (though calculations with a complete gA protein model have since revealed that anions remain unstable throughout the channel pore [32]). In accord with the suggestions of Urry, Roux showed using MD-free energy perturbation (FEP) of a simplified periodic gA-like β-helix model that cation/anion specificity of gA was caused by the asymmetric backbone charge distribution [33]. The amide groups, with their short N–H bond, are intrinsically less effective in stabilizing anions than the carbonyl groups, with their long C=O bond, are at stabilizing cations [33,34]. More recent evidence, originating with the solution of high resolution NMR structures, raises the possibility that the selectivity of cations over anions also may be attributable to the slight preferential alignment (tilt) of the carbonyl dipoles toward the interior of the pore lumen. This alignment would give rise to a negative electrostatic potential along the gA channel, as seen in continuum electrostatic calculations based on the (fixed) static NMR structure (e.g., Ref. [35]). However, as we have learned from permeation studies, one cannot always interpret mechanisms from a static picture as the significant flexibility of the protein is absent [20].

In this article, we use equilibrium sampling to determine a free energy profile for the permeation of monovalent cations (K^+) and anions (Cl^-) to determine the relative free energies of each ion as a function of position to help alleviate this uncertainty. In addition, we examine the permeation of divalent ions. X-ray scattering [36] and NMR [37–39] have shown that the divalent ions Ca^{2+} and Ba^{2+} are excluded from and weakly block gA just outside the narrow pore (~13 Å from the center of mass). The preferential binding of divalent cations outside the single-file pore of gA is indicative of the large hydration free energy (being almost four times that of K^+ [29]), and the associated tight binding to the hydration shells [40]. Divalent ions therefore maintain almost bulk-like first hydration shells that associate only with the carbonyl groups reaching furthest out from the channel entrance. The discrimination against divalent ion movement through the pore is likely determined by the absence of charged side chains in the protein [41] taken together with the much higher electrostatic barrier that would be expected for divalent cations, as predicted from the Born model for ion solvation. Given the challenge of accurately modeling the solvation of even a monovalent ion in this narrow pore with a fixed-charge force field, we seek to evaluate whether selectivity against divalent permeation can be observed in MD simulations via the PMF framework and present-day force fields. With care, MD-PMF calculations indeed can offer a

powerful tool for reproducing experiment and understanding the mechanisms of ion permeation and selectivity.

2. Methods and results

2.1. Molecular dynamics simulations

Dimyristoylphosphatidylcholine (DMPC) bilayers of different sizes (Fig. 2) were built around the gA protein using extensions of existing membrane-building techniques [42]. We simulated the gA helical dimer from Protein Data Bank PDB:1JNO [12], which has been shown to provide agreement with a range of experimental solution and solid state nuclear magnetic resonance observations [14]. The membranes consisted of ~1 or 3 shells of phospholipids, containing 20 or 96 lipid molecules (and 1080 or 3996 water molecules), respectively. Hexagonal periodic boundaries of respective xy-translation lengths 32.1 Å and 61.9 Å were imposed. Pressure coupling was employed in the z direction (parallel to the membrane normal, with average height ~75 Å, while the x–y dimensions of the box remained fixed. Ionic solutions of 1 M KCl were used to ensure good electrolyte sampling. Simulations were carried out with the program CHARMM [43] using the PARAM27
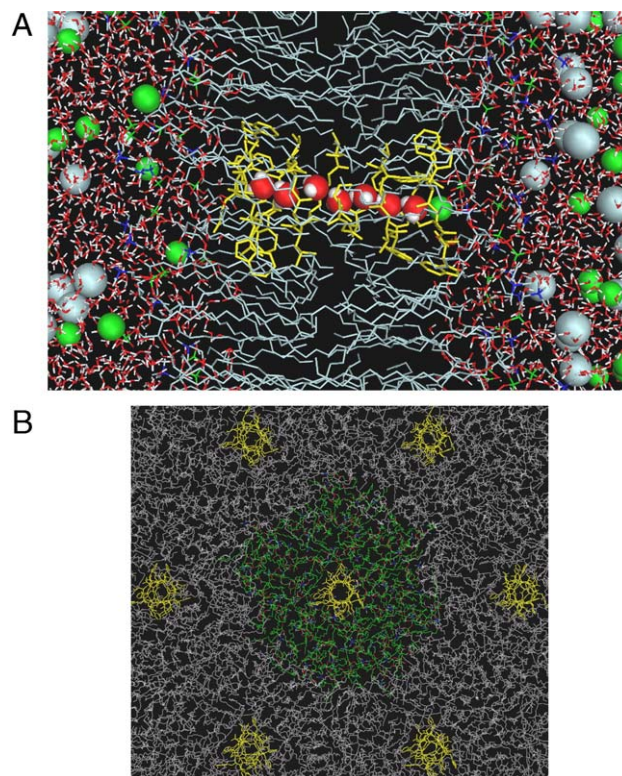

Fig. 2. Gramicidin A in a periodic bilayer: (A) 1 shell system: gA dimer (yellow); DMPC bilayer atoms C (gray), O (red), N (blue) and P (green); K^+ (green spheres) and Cl^- (gray spheres); water O (red) and H (white). Within the channel 7 single-file water molecules are drawn as spheres adjacent to a single K^+ at the channel entrance. Lipids from neighboring images are included in this figure. (B) 3 shell system (CPK color with green lipid C atoms) with hexagonal periodic images (CPK color with gray lipid C atoms) viewed along the membrane normal. Water molecules and ions have been removed for clarity. These images have been adapted from Ref. [27].

[44,45] protein/lipid force field with TIP3P water [46] parameters and ion Lennard Jones parameters from Beglov and Roux [47]. Simulations were also carried out with the all-atom amber PARAM94 [48] and united-atom GROMOS87 [49] force fields for comparison. With the AMBER94 force field, we employed the TIP3P water model and ion Lennard Jones parameters from Aqvist [50]. For the GROMOS87 force field, we employed the SPC water model [51] with ion parameters from Straatsma et al. [52]. Particle-mesh Ewald [53], SHAKE [54] and constant pressure and temperature algorithms [55] were employed in all simulations.

2.2. The potential of mean force

We calculate equilibrium potentials of mean force along reaction coordinates relevant to ion permeation by sampling in the CPT ensemble. The relevant order parameters are those deemed to describe slow processes. The most obvious of these are the coordinates of the ions as they translocate from one side of the membrane to the other under the action of a potential difference originating from a dispersed ionic gradient [56]. At high concentration, the pore maybe occupied by more than one ion, yet the 1-ion PMF, $\mathcal{W}(\mathbf{r}_1)$, will reveal much about the function of the gA channel. This 1-ion PMF can be evaluated as a configurational integral

$$e^{-\mathcal{W}(\mathbf{r}_1)/k_B T} = \frac{\int' d\mathbf{r}_2 \ldots \int' d\mathbf{r}_N \int d\mathbf{X} e^{-U(\mathbf{r}_1, \mathbf{r}_2, \ldots, \mathbf{r}_N; \mathbf{X})/k_B T}}{\int' d\mathbf{r}_2 \ldots \int' d\mathbf{r}_N \int d\mathbf{X} e^{-U(\mathbf{r}_1', \mathbf{r}_2, \ldots, \mathbf{r}_N; \mathbf{X})/k_B T}} \quad (1)$$

where k_B is Boltzmann's constant, T is the temperature, U is the potential energy as a function of ionic $\mathbf{r}_1$, $\mathbf{r}_2$, ..., $\mathbf{r}_N$ and all other degrees of freedom (water, protein, lipids) $\mathbf{X}$. The primes on the integrals indicate that ions $2-N$ reside in the bulk and we have chosen a reference $\mathcal{W}(\mathbf{r}_1') = 0$ at a position $\mathbf{r}_1'$ in the bulk. The 1-ion pore region has been determined to be defined approximately by a sphere of radius 14 Å [27] around the center of mass of the gA dimer. This is the largest sphere for which it is not possible to see two cations inside the pore region on one side of the channel. Furthermore, this sphere is almost devoid of anions, the first evidence of charge-based selectivity of the gA channel. With this choice of radius, it is possible to have one cation on each side of the channel (occurring 19% of the time in 1 M KCl solution [27]). To avoid this during the simulations, other ions (cations and anions) were excluded from this sphere with a repulsive flat-bottom spherical harmonic restraint with force constant 5 kcal/mol.

Because conduction is driven by a trans-membrane voltage difference, we choose a reaction coordinate z, parallel to the fixed membrane normal, that is the distance of the ion to the center of mass of the gA dimer. We may integrate over all lateral displacements to obtain a 1D PMF $W(z)$ [57].

$$e^{-W(z)/k_B T} \propto \int dx \, dy \, e^{-\mathcal{W}(x,y,z)/k_B T}. \quad (2)$$

Because such an integral will not be defined as the ion becomes unbounded (outside the channel), we restrict lateral

displacements with a flat-bottom cylindrical constraint of radius $R = 8$ Å and force constant 10 kcal/mol/Å^2 [26], represented by a Heaviside step function $H_{cyl}(x, y)$ that is 1 inside the bounding cylinder and 0 outside such that [27]

$$e^{-\mathcal{W}(z)/k_B T} = C \int dx \, dy \, H_{cyl}(x,y) e^{-\mathcal{W}(x,y,z)/k_B T}, \quad (3)$$

where C is a constant. By defining the 1D PMF to be zero in the bulk at $z = z'$ (e.g., $z' = 30$ Å), the constant C in Eq. (3) becomes

$$C = \frac{1}{\int dx \, dy \, H_{cyl}(x,y) e^{-\mathcal{W}(x,y,z')k_B T}}. \quad (4)$$

Because $\mathcal{W}$ becomes independent of x and y far from the channel (at $z = z'$), $\mathcal{W}(x, y, z') = \mathcal{W}(0, 0, z')$ and thus

$$C = \frac{e^{+\mathcal{W}(0,0,z')k_B T}}{\pi R^2} \quad (5)$$

which can be inserted into Eq. (3) to give

$$e^{-W(z)/k_B T} = \frac{1}{\pi R^2} \int dx \, dy \, H_{cyl}(x,y) e^{-[\mathcal{W}(x,y,z) - \mathcal{W}(0,0,z')]/k_B T}, \quad (6)$$

With such a restraint, the bulk reference has a definite value that is independent of the sampling time. We calculated this PMF with umbrella sampling [58] with 101 simulations, biased by window functions $w_i(z) = \frac{1}{2} K_i(z - z_i)^2$ (with $K_i = 10$ kcal/mol/Å^2) that hold the ion at 0.5 Å increments in $z = (-20, +30)$ Å. Initial configurations for PMF simulations were extracted from 4 ns of MD trajectory as previously described [27]. For each window, equilibration was carried out for 80 ps prior to trajectory generation for the PMF. Ionic distributions were then unbiased using the weighted histogram analysis method (WHAM) [59]. Long simulation times of 1–2 ns/window are needed in order to obtain reliable simulations. This is shown in Fig. 3 where the 1D PMF is calculated for different simulation time blocks spanning the total of 2 ns/window: 50 ps (40 curves in A), 100 ps (20 curves in B), 200 ps (10 curves in C), 300 ps (6 curves in D), 500 ps (4 curves in E) and 1 ns (2 curves in F) in the left hand column. Dotted vertical lines signify ±15 Å, approximately out to which the 1D PMF is defined. The asymmetry and variation in the PMFs is very large for 50 ps/window with the free energy on left and right sides of the channel varying from −8 to 8 kcal/mol, as measured at $z = \pm 15$ Å, and comparable to the height of the central barrier relative to these points. If one were to estimate the central barrier height, the results would be very different if the reference were on the left or right. The variation and asymmetry for 100 ps/window (B) is still very large (up to 8 kcal/mol). Calculations of the PMF based on such simulation times are clearly going to be in error. The magnitude of the asymmetry then drops to ~7, 5, 3 and 2 kcal/mol for 200, 300, 500 and 1000 ps/window, respectively. When the complete 2 ns is used in a single WHAM unbiasing (not shown), the asymmetry is <1 kcal/mol [27]. This asymmetry corresponds to a very small average force across the channel that can be removed by symmetrization where the WHAM equations are solved after creating duplicate windows on opposite sides of the
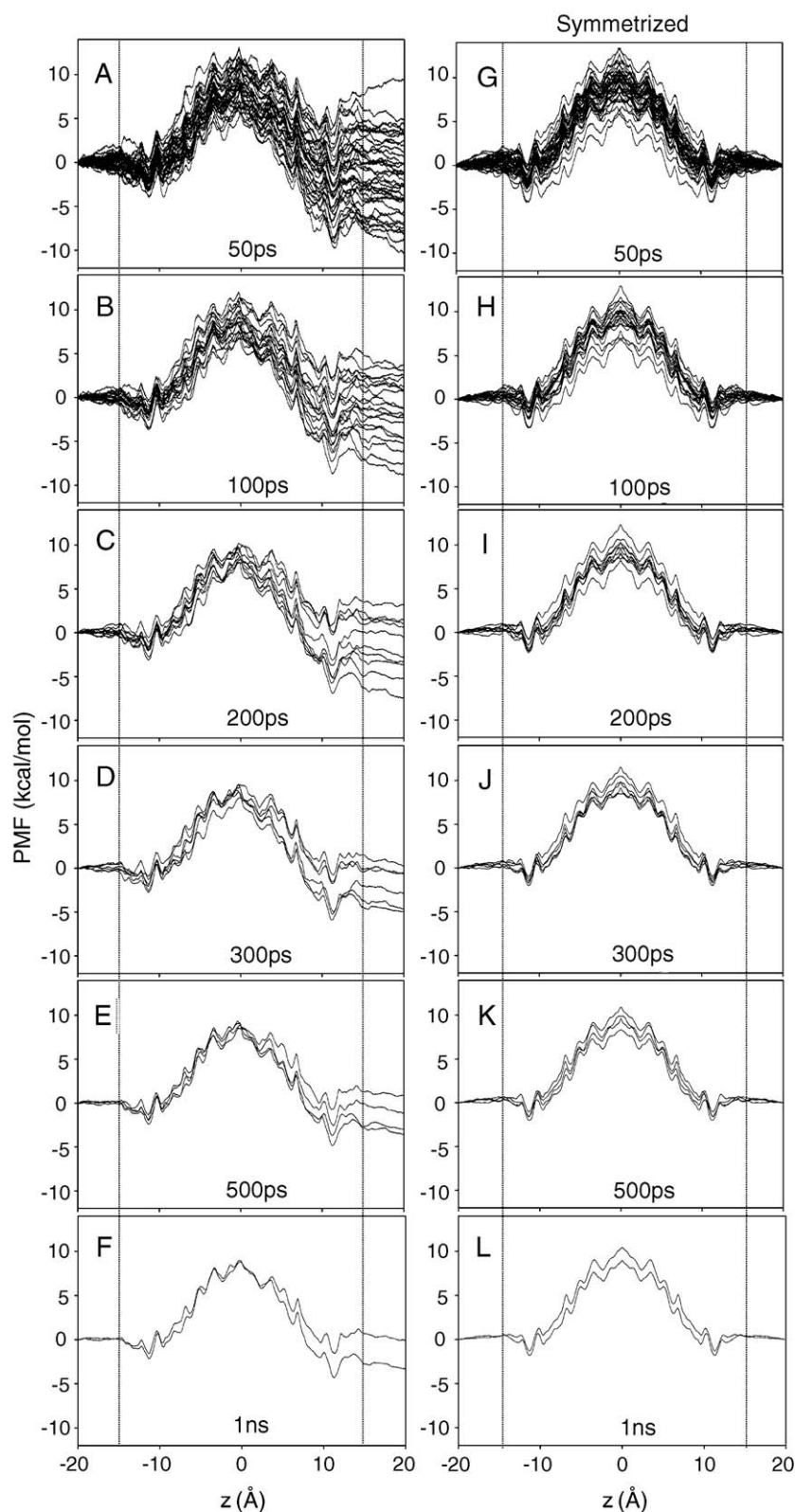
Fig. 3. 1D K$^+$ ion PMFs for the 1 shell system (20 lipids) and CHARMM27 force field (without artifact corrections) for different simulation times. (A–F) PMFs for all 50 ps–1 ns block samples in the total 2 ns simulation period per window. Each free energy profile has been matched at $z=-20$ Å. (G–L) The corresponding PMFs obtained by solution to the WHAM equations with A symmetrized biased density. Broken vertical lines at $|z|=15$ Å indicate approximately the bounds of validity of the 1D PMF.

channel. Fig. 4A shows the 1D PMF after 1 and 2 ns of simulation per window, deviating on average by just 0.3 kcal/mol, demonstrating good convergence. The symmetrized 1D PMF (after 2 ns) reveals a central barrier of ~ 11 kcal/mol with respect to the binding site (remembering that no barrier with respect to the bulk can be defined from this 1D profile). There is a deep outer binding site at $z = 11.3$ Å and a less deep inner binding site at 9.7 Å.

As a further check on the calculations, we have done calculations to examine the effects of the spherical constraint applied to both cations and anions, which was used to maintain a 1-ion pore. When we recalculated the PMF with a constraint on other cations only, leaving anions unbiased, the PMF was largely unaffected, with the inner and outer binding sites having unaltered depths but with a small shift toward of the inner site by 0.3–0.4 Å toward the channel center and no observed change in the outer binding site location. This lack of significant change is to be expected because anions are almost completely excluded from the channel without the constraint. We also recalculated the PMF without any umbrella sampling bias, instead holding an ion inside the range 7.5–13.5 Å, and found that the inner and outer binding site positions and depths were approximately reproduced. When we recalculated the PMF without the lateral restraint that was used to provide a well defined region in the bulk for the ion, we observed no noticeable changes in the PMF within the pore, but found that the PMF drops steadily as the ion departs the channel, as expected.
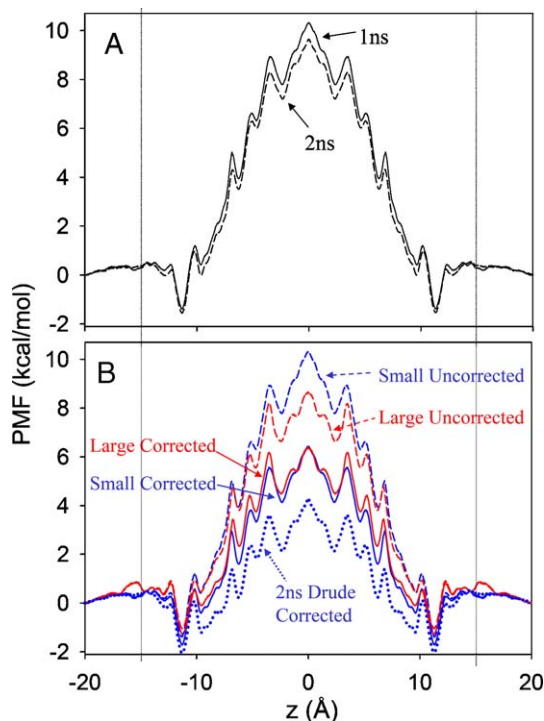

Fig. 4. (A) Symmetrized 1D K^+ ion PMFs (without artifact corrections) for the small system (20 lipids) from the first 1 ns (solid curve) and complete 2 ns/window (dashed curve). (B) Comparison of K^+ ion PMFs, before and after corrections, between small (20 lipids, red) and large (96 lipid, blue) membranes, matched at $z = 20$ Å. These plots have been adapted from Ref. [27]. The best estimate of the PMF, shown as a dotted curve, is that from 2 ns/window simulation with the Drude-based correction.

Though apparently reliable, there are systematic errors in the predicted energetics in the simulated atomic model. A spurious destabilization of the ion is caused by periodicity (length L) of the system. In addition, lipid hydrocarbon chains have a dielectric constant of 1 [60,101], which does not adequately model bulk hydrocarbon with dielectric constant ~ 2 [61]. These artifacts can be corrected using continuum electrostatics [26, 62] using a thermodynamic cycle discussed in detail in Ref. [27]. The corrected PMF $W_{corr}(z; \epsilon_m = 2; L = \infty)$, with membrane dielectric constant, $\epsilon_m = 2$, and for an infinite membrane with no periodic effect, maybe related to the uncorrected MD-PMF $W_{MD}(z; \epsilon_m = 1; L = L_0)$ by

$$W_{corr}(z) = W_{MD}(z) + \Delta G_{diel}(z) + \Delta G_{size}(z), \qquad (7)$$

where

$$\begin{aligned} \Delta G_{diel}(z) =& \Delta G(z; \epsilon_m = 1 \to 2; L = \infty) \\ &- \Delta G(z'; \epsilon_m = 1 \to 2; L = \infty) \end{aligned} \qquad (8)$$

and

$$\begin{aligned} \Delta G_{size}(z) =& \Delta G(z; \epsilon_m = 1; L = L_0 \to \infty) \\ &- \Delta G(z'; \epsilon_m = 1; L = L_0 \to \infty). \end{aligned} \qquad (9)$$

We solved the finite-difference Poisson equation using a set of 50 instantaneous configurations of the protein and its water contents from umbrella sampling windows, as previously described [27]. These estimates show that correcting for the spurious destabilization due to periodicity leads to a -1.6 kcal/mol correction (for monovalent ion at the channel center, relative to the bulk) for the small system (Fig. 5A). For the large system, the correction for periodicity had a maximum amplitude of 0.03 kcal/mol and is not plotted. Correcting for the effect of the dielectric constant of the hydrocarbon chains leads to a further -2.1 kcal/mol stabilization at the channel center (Fig. 5B). We also estimate that the effect of reducing the salt concentration [63] from 1 M to a level of 0.1 M (better corresponding to the single-ion regime [26]) is approximately -0.2 kcal/mol at the channel center. Fig. 4B shows that the K^+ PMF barrier (for the small system after 1 ns of simulation per window) after all of these corrections is reduced to ~ 8.1 kcal/mol, with respect to the deepest point (the outer binding site).

To estimate the magnitude of the dielectric correction from a different approach, we have performed calculations using a polarizable force field on hydrocarbon chains based on Drude oscillators [64], as reported previously [26] and similar to previous calculations employing polarizability [65]. In this case, the change in the stabilization of the ion was -3.6 ± 0.3 kcal/mol, a little larger than the MD averaged Poisson solution value of -2.1 kcal/mol. This apparent underestimation of ΔG_{diel} led us to adjust the original correction curve of Fig. 5B by scaling the dielectric correction by a factor of 3.6/2.1. We shall refer to PMFs corrected with this scaled correction as the "Drude corrected" PMF, as shown in Fig. 4 (dotted curve) for the 2 ns PMF. With this correction applied, the barrier is now only 6.6 kcal/mol relative to the binding site. Finally, to test the accuracy of our size correction of Fig. 5A and to demonstrate
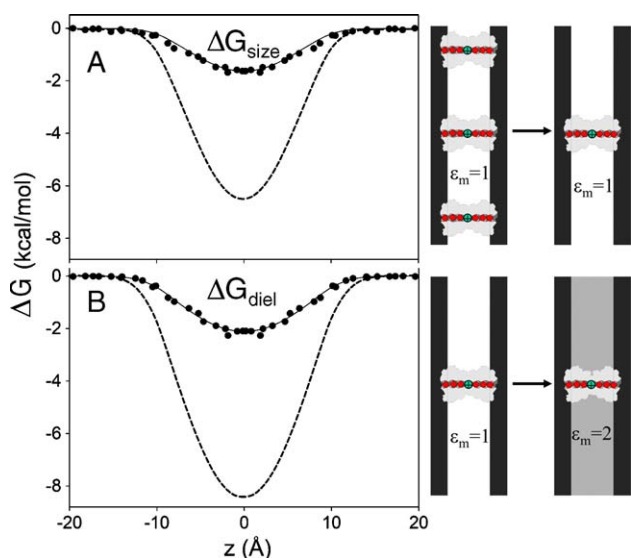
Fig. 5. Corrections applied to the 1D PMF to correct for simulation artifacts. (A) Poisson size correction (1 shell of lipids→infinite bilayer), (B) Poisson membrane dielectric constant correction ($\epsilon_m=1\rightarrow2$). Data points represent MD ensemble averaged Poisson solutions. The solid curves are single MD-average structure Poisson solutions using best-fit dielectric constants, as described in Ref. [27]. Steps in the free energy cycle are illustrated on the right. The gA channel is shown as yellow, high dielectric ($\epsilon=80$) bulk water as blue, membrane core with $\epsilon=1$ as white, membrane core with $\epsilon=2$ as gray, pore water molecules as red (O) and white (H) circles, and K^+ as green circles with '+' sign. Dotted curves are for the Ca^{2+} based on single Poisson solutions using fitted dielectric constants for the monovalent ion. (For interpretation of the references to colour in this figure legend, the reader is referred to the web version of this article.)

consistency of the results, Fig. 4B compares the small and large system PMFs (using 1 ns/window) before corrections as dashed curves. In the solid curves of Fig. 4B all corrections (size, dielectric and concentration) have been applied resulting in very similar PMFs that differ on average by just 0.28 kcal/mol, demonstrating the accuracy of the Poisson correction scheme.

2.3. Contact with experimental observables

Experimental binding and conductance observables may be obtained directly from the calculated MD-PMFs. The stationary K^+ flux (J) across the channel can be determined from a 1D Nernst–Planck equation [66]

$$J = -D(z)\frac{dP(z)}{dz} - P(z)\frac{D(z)}{k_BT}\frac{dW_{tot(z)}}{dz}, \qquad (10)$$

where $D(z)$ is the K^+ diffusion coefficient and $P(z)$ is the spatial probability density of K^+. W_{tot} is a sum of the equilibrium PMF, W, and the interaction of all atomic charges, q_i, with the transmembrane potential, ϕ_{mp}. This interaction can be re-expressed in terms of a coupling to the dipole moment of system via a cumulant expansion of the form [57]

$$W_{tot}(z) \approx W(z) + q_{ion}\phi_{mp}(z)\langle\Delta\mu(z)\rangle\frac{d}{dz}\phi_{mp}$$
$$- \frac{1}{2k_BT}\langle\Delta\mu^2(z)\rangle\left(\frac{d}{dz}\phi_{mp}\right)^2, \qquad (11)$$

where $\Delta\mu(z)=\mu(z)-\langle\mu(z)\rangle$, determined from biased trajectories, and ϕ_{mp} is obtained by solving the modified Poisson–Boltzmann equation [57]. The sum of all terms representing the coupling of the system charge distribution to the applied voltage difference is shown in Fig. 6A (with the uncorrected transmembrane potential superimposed as thin curves). When 100 mV is applied (solid curves in Fig. 6), the linear and quadratic corrections remain under 0.15 and 0.04 kcal/mol, respectively. At 500 mV (dash-dot curves), these corrections approach 1 kcal/mol; thus having a considerable effect on the conductance. At lower voltages (comparable to the cell membrane potential), the effect of the membrane potential on the total PMF can be neglected. In such a regime, the maximum conductance is given by [67]

$$g_{max} = \frac{e^2}{k_BTL_p^2}\langle D(z)^{-1}e^{+W(z)/k_BT}\rangle^{-1}\langle e^{-W(z)/k_BT}\rangle^{-1} \qquad (12)$$

where the brackets signify spatial averaging over the length of the pore region. Because the maximum conductance corresponds to the high concentration limit, a formalism based on a single-ion PMF alone only provides an order of magnitude estimate because it neglects the effects of multiple occupancy [68]. We have calculated $D(z)$, required in Eq. (12), by separating dissipative and systematic forces using a method based on the Laplace transform of the velocity autocorrelation function, employing an analysis of the generalized Langevin
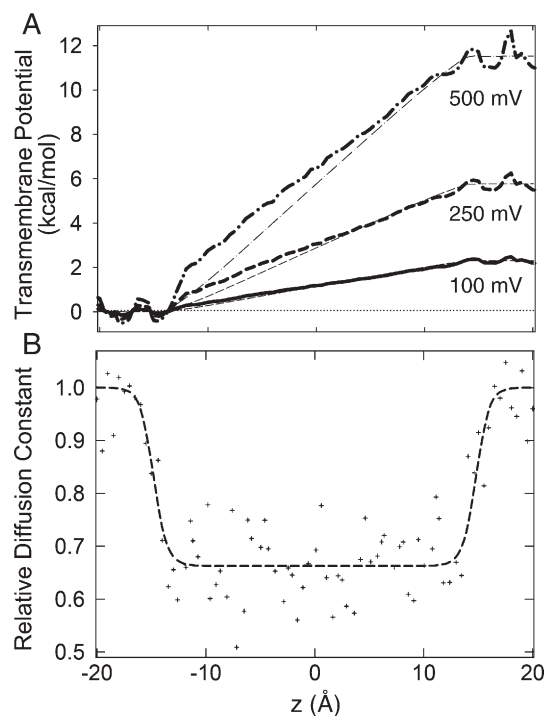

Fig. 6. Terms in the cumulant expansion Eq. (11). (A) The membrane potential $q_{ion}\phi_{mp}$ for 100 mV (solid), 250 mV (dashed) and 500 mV (dash-dot) applied potential difference from solutions to the modified Poisson–Boltzmann equation with MD-averaged structure are plotted as thin curves. The linear dipole and quadratic dipole cumulant corrections are added to produce the thick curves. (B) K^+ axial diffusion profile, relative to the bulk value of 0.37 Å^2/ps. The fit (dashed line) is a sigmoidal function. Adapted from Ref. [27].

equation for a harmonic oscillator [69,70], as described previously [27]. Fig. 6B reveals that $D(z)$ is ~2/3 of bulk diffusion coefficient within the channel.

Using Eq. (12), the maximum conductance based on the corrected 1 ns PMF (solid blue curve) of Fig. 4B is 0.81 pS, while based on the 2 ns/window PMF of Fig. 4A (following artifact corrections, not shown) the g_{max} is 1.54 pS, approximately one order of magnitude less than the experimental value of 21 pS (in DPhPC bilayers with 1 M KCl at 100 mV [71]). When we account for the underestimation of the Poisson correction for lipid chain dielectric constant by using the Drude oscillator corrected PMF (dotted curve in Fig. 4B), we obtain a maximum conductance of 9.3 pS, which is only a factor of 2 away from the experimental value. This indicates that our best estimate of the PMF for K^+ conduction is likely to be within a kcal/mol of the true free energy profile.

The single-ion dissociation constant K_D can be expressed in terms of the three-dimensional PMF, $\mathcal{W}(\mathbf{r})$ [57]

$$K_D^{-1} = \frac{\int d\mathbf{r}\ \mathcal{H}_{site}(\mathbf{r}) e^{-\mathcal{W}(\mathbf{r})/k_B T}}{e^{-\mathcal{W}(\mathbf{r}')/k_B T}}, \tag{13}$$

where $\mathbf{r}'$ is a reference position in the bulk and where the binding site is defined by the Heaviside step function $\mathcal{H}_{site}(\mathbf{r})$, which is 1 inside the binding site and 0 outside. K_D may also be expressed in terms of the 1D PMF, $W(z)$, as long as the sampling of the lateral motion (i.e., with a cylindrical restraint) and corresponding offset constant are handled correctly [26]. We define the binding site to be within the range $z_{min} \leq z \leq z_{max}$ in the axial direction

$$\mathcal{H}_{site}(\mathbf{r}) = h_{site}(z) H_{cyl}(x,y), \tag{14}$$

where

$$h_{site}(z) = \begin{cases} 1; & z_{min} \geq z \geq z_{max} \\ 0; & z < z_{min} \\ 0; & z > z_{max} \end{cases}, \tag{15}$$

then, with $\mathbf{r}' = (0, 0, z')$, Eq. (13) becomes

$$K_D^{-1} = \int dx\ dy\ dz\ \mathcal{H}_{site}(x,y,z) e^{-[\mathcal{W}(x,y,z) - \mathcal{W}(0,0,z')]/k_B T} \tag{16}$$

$$= \int dz\ h_{site}(z) \int dx\ dy\ H_{cyl}(x,y) e^{-[\mathcal{W}(x,y,z) - \mathcal{W}(0,0,z')]/k_B T}. \tag{17}$$

Then, using Eq. (6), we find the relationship between the dissociation constant and the 1D PMF

$$K_D^{-1} = \pi R^2 \int dz\ h_{site}(z) e^{-W(z)/k_B T} \tag{18}$$

$$= \pi R^2 \int_{z_{min}}^{z_{max}} dz\ e^{-W(z)/k_B T}, \tag{19}$$

where R is the radius of the bounding cylinder used to calculate the 1D PMF. We calculate a dissociation constant for the

channel of 0.30 M using the corrected 1 ns PMF and a value of 0.21 M using the 2 ns/window PMF from Fig. 4A. Recalculation using the Drude-corrected 2 ns/window PMF (dotted curve in Fig. 4B) yields a value of 0.14 M, in agreement with experimental values from NMR and conductance studies: 0.07 M [19] (in diphytanoylphosphatidylcholine/n-decane bilayers), 0.017 M [73] (measured in dodecylphosphocholine micelles), 0.019–0.73 M [74] (in aqueous lysophosphatidylcholine dispersions) and 0.035 M [75] (in glycerylmonoolein bilayers). We have also determined that the ion preferentially binds to the outer binding site ($10.2 < z < 12.5$ Å) with $K_D = 0.83$ M as compared to the inner site ($6.9 < z < 10.2$ Å) with $K_D = 3.6$ M. This is in agreement with the observations of Tian and Cross [39] who observed a larger chemical shift for the Leu12–Trp13 than the Leu10–Trp11 linkage for K^+. It is, however, in contrast to the observations of X-ray scattering by Olah et al. [36] who see preferred binding nearer the inner site.

2.4. Force field dependence

The obvious difficulty of accurately representing interactions of ions with bulk water, pore water and protein led us to investigate the effect of the choice of force field on the PMFs and calculated observables. We aim to explore the robustness of our calculations and determine how sensitive the observables are to the precise values of interaction parameters. Table 1 summarizes calculations of gas phase water and N-methyl-acetamide (NMA) interactions, as well as hydration free energies in bulk water and charging free energies in bulk NMA. The results for ion–water interaction energies and solvation free energies are all in approximate agreement, irrespective of the chosen force field. We note, however, that there is considerable uncertainty in the experimental value for the hydration free energy of K^+ [76]. There is also some

Table 1
Interaction energies with gas phase water and NMA and solvation free energies in liquid water and NMA (absolute values) for different force fields, extended from [27]

Force field	(Interaction in gas phase)		(Solvation in liquid phase)	
	K-water	K-NMA	K-water (solvation)	K-NMA (charging)
	Absolute energies (kcal/mol)			
Experiment	17.9	28.3–32.3	79.3[1]	–
Ab initio	15.9–17.6	24.8–31.7	–	–
CHARMM27	18.9	24.2	81.5[2]	89.2
CHARMM27−	18.9	21.6	81.5[2]	82.0
CHARMM27+	18.9	26.5	81.5[2]	97.6
AMBER94	18.2	23.7	80.9[3]	81.8
GROMOS87	17.8	16.6	77.2[4]	71.6

Values for gas phase interactions with water and NMA have been taken from Ref. [99]. Values for liquid water are solvation free energies (including cavity contribution) taken from: (1) Noyes [100], (2) Beglov and Roux [47], (3) Aqvist [50] and (4) Hummer et al. [77]. The value from Hummer et al. has been adjusted for the air–water interfacial potential (see text). In comparison, values for liquid NMA are charging free energies only from Allen et al. [27]. CHARMM27 is the unmodified CHARMM force field with $\sigma_{KO} = 3.46$ Å, CHARMM27+ has a strengthened K–O interaction with $\sigma_{KO} = 3.30$ Å and CHARMM27− has a weakened K–O interaction with $\sigma_{KO} = 3.69$ Å.

uncertainty in the GROMOS87 value using the Straatsma and Berendesen ion parameters because the original calculations were based on cutoffs and employed a Born correction to obtain very poor agreement with experiment. We instead quote the more recent estimate based on the parameters used by Hummer et al. [77] and correct for the absence of an air–water interfacial potential in the Ewald summation approach to long-ranged electrostatics by adding 12.5 kcal/mol to the absolute value of the hydration free energy [76]. The results for the ion interaction with gas and liquid phase NMA are quite sensitive to the choice of force field. The gas and bulk phase energetic quantities are difficult to reconcile with a fixed force field [78,79]. This table reveals that while CHARMM27 and AMBER94 come close to representing the gas phase and bulk solvation free energies for the ion with NMA, GROMOS87 yields a gas phase interaction that it ~ 8 kcal/mol too positive, indicating a very non-polar protein. Furthermore, the difference between the charging free energies in bulk NMA for CHARMM27 and AMBER94 of 7.4 kcal/mol symbolizes the sensitivity to the parameterization. We will see in the following section that the protein is responsible for up to half of the ion's solvation free energy within the channel such that the difference in ion–protein interactions will have a considerable impact on the equilibrium PMF.

Fig. 7A compares the artifact-corrected PMFs calculated with CHARMM27, AMBER94 and the united-atom GROMOS87 force fields with calculated observables listed in Table 2. It is clear that GROMOS87 is unable to describe ion permeation in this

Table 2
Calculated maximum conductances and dissociation coefficients for CHARMM27, AMBER94 and GROMOS87 force fields, as well as variations of CHARMM27, as reported in Ref. [27]

	g_{max} (pS)	K_D (mol/l)
Experiment	21[a]	0.017 M[b], 0.019–0.73 M[c], 0.035 M[d], 0.07±0.01 M[e]
1 ns/window		
CHARMM27	0.81	0.30
CHARMM27−	0.026	5.8
CHARMM27+	0.54	0.0015
AMBER94	6.9	2.4
GROMOS87	0.0069	2.8
Drude corrected CHARMM27	5.1	0.21
Drude corrected AMBER94	28.1	1.6
Drude corrected GROMOS87	0.050	2.6
2 ns/window		
CHARMM27	1.54	0.21
Drude corrected CHARMM27	9.27	0.14

Experimental measurements: [a][71], [b][73], [c][74], [d][75] and [e][19].

narrow channel with a large central barrier, almost nonexistent binding and 4 orders of magnitude too little conductance. However, both AMBER94 and CHARMM27 have significantly lower barriers and differ, on average, by only 1.0 kcal/mol. AMBER94 has an improved g_{max} of 6.9 pS, as compared to 0.81 pS for K$^+$, but exhibits too little binding compared to experiment. However, both CHARMM27 and AMBER94 predict results to within almost an order of magnitude of both experimental conductance and binding data. This approximate quantitative agreement is improved with the use of Drude oscillator-based corrections, as shown in Table 2, revealing marginally better results for the CHARMM27 force field, is most encouraging. The different shapes of the AMBER94 and CHARMM27 emphasize the sensitivity of the detailed shape to subtle differences between these all-atom, but non-polarizable force fields.

To further explore the sensitivity of results on the parameterization, we have investigated the effects of small changes in ion–protein interaction potentials. To set a range for these changes, we compare to ion–NMA gas phase interaction energies and also the free energy of charging of K$^+$ in liquid NMA, which should be similar to that in liquid water [34]. If one matches to the gas phase interaction, the solvation free energy in bulk will be significantly overestimated; if one matches the bulk value, the gas phase interaction will be too weak. Ultimately, there should be a point where the force field does a best job of finding a compromise between gas phase and bulk representations. Without atomic polarizability, it is very difficult to get both of these quantities right. The CHARMM27 force field gives a K$^+$-liquid NMA free energy ~ 7 kcal/mol more negative than the K$^+$-bulk water free energy and an NMA gas phase interaction slightly less than the lower bound of the ab initio result. One can explore this range by modifying the ion–protein Lennard Jones parameter, as done previously [78]. The first modification, called CHARMM27− (weaker interaction), produces a liquid NMA charging free energy of 82.0 kcal/mol, similar to that of bulk water [80], and a gas phase interaction of
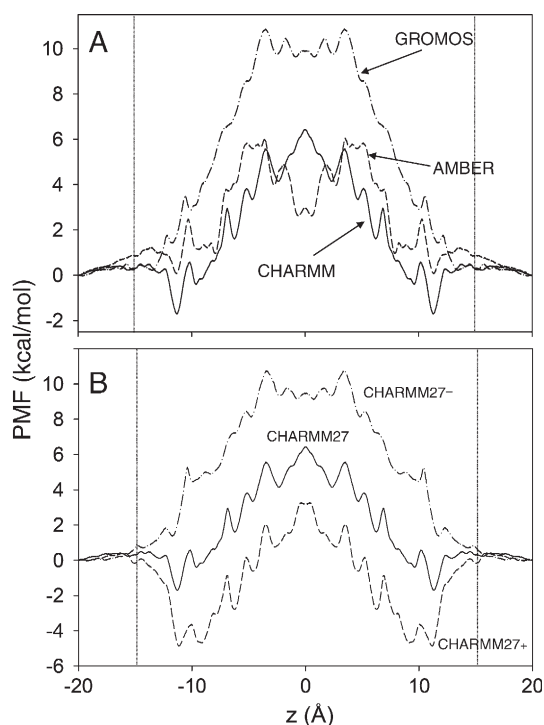

Fig. 7. (A) One-dimensional K$^+$ ion PMFs using the CHARMM27, AMBER94 and GROMOS87 force fields. (B) One-dimensional K$^+$ ion PMFs using the CHARMM27 force field and variations CHARMM27+ (dashed) and CHARMM27− (dash-dot). Both graphs have been adapted from Ref. [27]. All PMFs have been calculated from 1 ns/window simulations and have been corrected for simulation artifacts.

21.6 kcal/mol (significantly less than experiment). The second modification, called CHARMM27+ (stronger interaction), produces a gas phase interaction energy of 26.5 kcal/mol, within the ab initio range and near the lower experimental bound. The charging free energy in bulk NMA with CHARMM27+ is 97.6 kcal/mol, around 16 kcal/mol more than the estimated experimental value. This demonstrates the rather extreme sensitivity of energetics to small 0.1–0.2 Å changes in only one parameter (the ion-carbonyl oxygen Lennard Jones σ) and we therefore expect considerable differences in the calculated PMFs.

The PMF obtained with the CHARMM27+ force field is shown as a dashed curve in Fig. 7B. Because the parameter was chosen to approximately reproduce the gas phase K$^+$-NMA interaction energy, the central barrier in the PMF is reduced and the depths of the binding sites increased (and the inner and outer sites have become of similar depth, due to the increased involvement of the protein carbonyls at the inner binding site, as revealed in the following section). In contrast, the PMF obtained with the CHARMM27+ force field, is shown as a dash-dot curve in Fig. 7B, reveals a dramatically increased central barrier due to the matching to the ion charging free energy in liquid NMA to that of bulk water. The barrier for CHARMM27– is almost 11 kcal/mol and the binding sites have almost vanished due to the less attractive interaction between the ion and the protein. We have computed maximum conductances and dissociation constants using these two variations of the force field parameters in Table 2. The CHARMM27+ PMF leads to a lower g_{max} than the unmodified CHARMM27 PMF and to a dissociation constant is at least an order of magnitude too low. The CHARMM27– PMF also is not providing any improved agreement with experiment, with almost no binding and 3 orders of magnitude too low conductance. This reinforces the success of the unmodified CHARMM27 force field to provide a good compromise between gas and liquid phase solvation in the absence of many-body effects.

2.5. Mechanisms of permeation

We have presented results for the 1-ion, 1D PMF and established a connection with experimental observations of binding and conductance within this 1D framework. The 1D PMF, however, cannot connect the pore and bulk electrolyte regions because it is undefined outside the pore. Distributions, biased in z, involving a second variable r, may be unbiased to produce a 2D PMF $W(z, r)$ as a function of axial and radial positions [27]. The calculated PMF in the vicinity of the pore region is shown in Fig. 8A (for a greater range of axial and radial variables, see Ref. [27]). This (uncorrected) 2D PMF reveals the positions and relative free energies of binding sites and the central barrier experienced by the permeating ion, as well as the extent of lateral ion motion. Because the 2D PMF is determined in the laboratory frame, lateral ion movement and channel tilting (12° on average [26]) has led to broad entrances in the 2D PMF. The outer binding site at $z=11.3$ Å is the deepest point in the free energy surface, being −3.2 kcal/mol relative to the bulk. In the narrowest part of
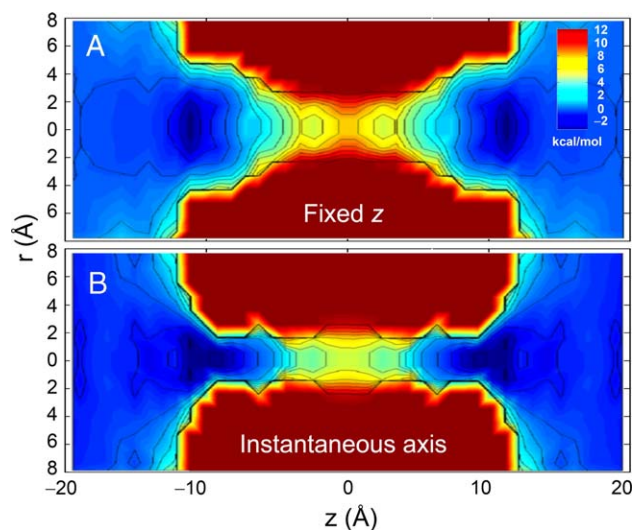

Fig. 8. Two-dimensional K$^+$ ion PMFs in the pore region for two different reaction coordinates: (A) projection of the distance to the center of mass onto the membrane normal, z, and (B) the position along the instantaneous (time-varying) channel axis; similar to that in Ref. [27]. Each surface is based on a calculation with a symmetrized biased density using the first 1 ns of simulation.

the channel, an ion experiences a barrier of 7.2 kcal/mol relative to the bulk. This barrier has been confirmed to be accurate to the order of ~1 kcal/mol with free energy perturbation calculations [26].

The wide entrances in the 2D PMF of Fig. 8A led us to wonder what the PMF may look like if we had followed an instantaneous axis through the ion channel rather than one fixed in the laboratory frame. Although the trans-membrane coordinate is pertinent to ion conduction, an instantaneous frame PMF should reveal in more detail the ion–protein–water interplay. We carried out umbrella sampling along a coordinate that is the distance of the ion from the center of mass of the channel dimer, projected onto the axis connecting the centers of mass of the two monomers. The resulting 2D PMF is shown in Fig. 8B. The shape is markedly different, now having no wide 'free energy vestibules' as seen in Fig. 8A. Interestingly, the outer binding sites are now seen to be off-axis, as previously suggested experimentally [81]. This is understandable because the ion is outside the single-file region where it is hydrated by 3 water molecules (in contrast to the inner site where it is in the single-file region and hydrated by just 2 water molecules) as shown below. Finally, the inner binding sites (−3.5 kcal/mol) are in fact deeper than the outer sites (−3.0 kcal/mol) in the instantaneous-axis 2D PMF, whereas they were almost nonexistent (−0.5 kcal/mol) in the fixed-frame 2D PMF. It is because the outer binding sites are off-axis, and therefore occupy a greater volume, than the 1D PMF has a global minimum there. The observed off-axis binding implies greater translational freedom such that the protein backbone will require less distortion to stabilize the ion.

In 1984, Mackay et al. identified a possible key role of the single-file water to overcome the large dehydration barrier [82]. They conjectured that water molecules aligned in single file in

the narrow were more able to solvate an ion than water molecules in the bulk phase. We have resolved the contributions to the overall PMF describing ion permeation from components, α, of the system [56],

$$W_\alpha(z) = W_\alpha(z_0) - \int_{z_0}^{z} dz' \langle F_\alpha(z') \rangle. \tag{20}$$

One possible mean force decomposition is shown in Fig. 9 where it can be see that the relatively flat PMF requires almost complete cancellation of very large opposing contributions from protein, single-file water and the bulk electrolyte and membrane; highlighting the challenge of studying permeation through a narrow pore. The contribution from the membrane and bulk electrolyte is 67.4 kcal/mol, as expected for a Born energy barrier due to a low dielectric membrane slab [83,84]. Surprisingly, the single-file water alone accounts for -39.2 kcal/mol stabilization which is nearly half of the bulk hydration free energy [34] and approximately equal to the interaction energy with the entire first bulk hydration shell [85], which can be attributed to the strong preferential alignment of the water in the narrow pore.

The complexity and importance of ion hydration highlights the need for an accurate description of the interactions with ions in the narrow pore. The non-polarizable TIP3P water model [46], though it succeeds to capture many features of the bulk liquid, was not parameterized to describe such a situation. To understand better the possible errors, we calculated the charging free energy of a K^+ at the center of a model system comprising 8 water molecules in single file using non-polarizable TIP3P as well as the polarizable SWM4-DP [64] water model based on Drude oscillators. Using TIP3P, the charging free energy was -42.0 kcal/mol, while that for SWM4-DP was -41.5 kcal/mol. Including the influence of a cavity reaction field, representing bulk water, the charging free energies became -52.2 and -52.3 kcal/mol, respectively. We conclude that the non-polarizable TIP3P water model adequately describes both ion interactions with bulk water as well as the single-file water in the narrow pore.

Th large stabilization that results from interactions with the single-file pore water led us to question whether the kinetics of
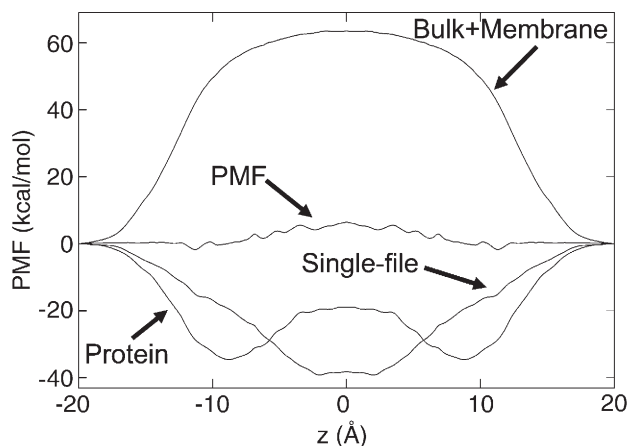

Fig. 9. Mean force decomposition from [26]. Average forces have been anti-symmetrized before integration with Eq. (20).
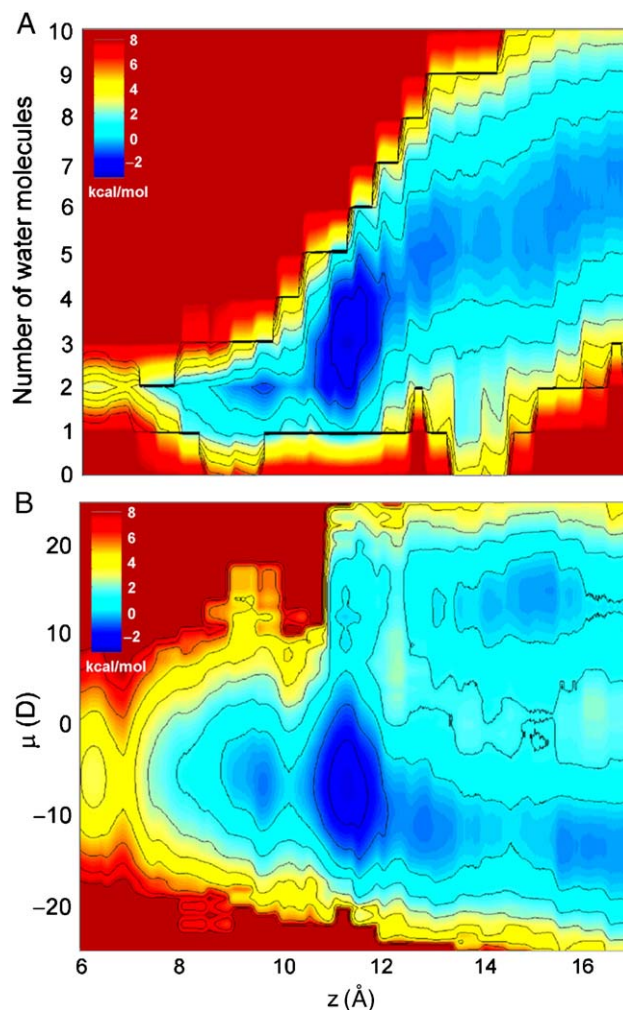

Fig. 10. (A) 2D PMF $W(z, n)$ as function of K^+ ion z and hydration number n. (B) 2D PMF $W(z, \mu)$ as a function of position and single-file water dipole moment $\mu(B)$. Modified from [26].

hydration could be rate determining in the ion association with the pore. For example, if the ion must wait at a particular position for dehydration to occur, then this could suggest that an additional dehydration order parameter may be needed to describe the permeation process [86]. The 2D PMF $W(z, n)$ of Fig. 10A shows the free energy of an ion at z, hydrated by n water molecules in the first shell, relative to $z = 30$ Å where $n \sim 6$–7 (in agreement with the calculated bulk hydration number of 6.46 in 1 M KCl [87]). Dehydration seems to be a continuous process over the range of ion positions from outside to inside the narrow pore, dropping to 3 in the outer site and 2 in the inner binding site, at no point experiencing a noticeable free energy barrier as a function of n.

Work is required to flip the orientation of the single file of water molecules inside the narrow pore [88]. Because ion movement necessitates a corresponding alignment of the water column (with oxygen end of chain facing the approaching cation), one can immediately envision an entrance barrier associated with chain flipping. Fig. 10B shows the 2D PMF, $W(z, \mu)$, as a function of the ion position and the net dipole moment of the single-file water molecules. When the ion is

outside the channel there are two possible dipole moments for the single file, ± 15 D, corresponding to the water molecules dipoles running almost parallel or anti-parallel to the z-axis, with corresponding free energy troughs in the 2D PMF surface. The bi-modality of the 2D distribution outside the channel continues into the outer binding site where it is still possible to have a water column in either orientation. When the ion occupies this site, the preferred state has the water at the end of the single-file column with its oxygen pointing toward the cation ($\mu = -15$ D). If the ion approaches a pore with the dipole at $+15$ D, the ion will not be able to enter the channel. There is a 2–3 kcal/mol barrier to flip the column while the ion is outside the channel, in agreement with a previous estimate of 2.2 kcal/mol [88]. An alternative conduction route is for the ion to enter the outer binding site and then overcome a smaller barrier of <1 kcal/mol to flip the single-file. This sudden change in μ has revealed a free energy barrier opposing permeation that is not a function of the coordinate z. To integrate over the equilibrium distribution of water column orientations for every ion position would require of the order of ns sampling, explaining the noisy PMF in the bulk in Fig. 10B. Any PMF that uses only a single positional order parameter as a reaction coordinate and samples for a time shorter than this is likely to be in error. In such a case, 2 order parameters would be needed to describe ion permeation (z and μ), which would be incompatible with the 1D Nernst–Planck Eq. (10) theory employed here, or any conduction model based on ionic positions alone.

The dipole moment of the single-file water creates a complication with regards to the coupling to the external potential difference, as we have seen (c.f. Fig. 6), and will also in addition introduce a complication for multiple ion mechanisms that will be significant at high concentrations. As an ion approaches from the right in Fig. 10B, it requires a dipole moment of -15 D to enter. Once it crosses, the chain of waters will have been zipped up leaving the dipole moment at $+15$ D, making it difficult for another ion to enter from the right. This suggests that there may be a structural long-range coupling across the pore, which would be absent in continuum solvent models.

2.6. Valence selectivity

To understand better the channel's valence selectivity, we determined PMFs for the permeation of the anion Cl^- and divalent cation Ca^{2+} through gA. In the process of computing PMFs for these ions, we encountered phenomena not seen for the monovalent cation case. Fig. 11A shows a typical configuration of protein and water molecules when a K^+ is held deep inside the channel during umbrella sampling (following 1 ns of simulation). It can be seen that a fairly uniform single file of water is maintained, a situation that is typical for all ion positions throughout the channel. When the K^+ is near the center, adjacent to the N-termini of each gA monomer, occasionally, a third water may be seen adjacent to the ion (Fig. 11B), yet the water column and protein are well maintained.

By comparison, Fig. 11C and D reveal how the hydration and protein can change in the presence of a Cl^- which is held

there for 1 ns of simulation. Panel C shows that additional waters are crowding around the anion to stabilize it, presumably because the backbone of gA is unable to solvate Cl^- effectively. In fact, the anion has moved outside of the pore in this instance. The movement of the ion outside of the pore occurred primarily in the region near the C-terminal end of the helix (for approximately $|z| > 8$ Å) and near the center of the channel where the two monomers join by H-bonding (for approximately $|z| < 3$ Å). For the most part, however, the anion remained within the channel pore, but with additional waters crowding around the ion. Near the channel center this "disruption" can be more severe, as shown in Fig. 11D, where the additional water tends to bend the gA channel. Situations, such as those illustrated in C and D, were never observed with K^+. We carried out additional simulations with artificially constrained backbones in an attempt to reduce the protein-perturbing effects deep in the channel. Umbrella sampling simulations with constraints on backbone atoms of 1 and 10 kcal/mol/Å^2 were carried out. In these cases, the protein-disrupting effects of the anion were drastically reduced. In almost every window, the single-file water column was maintained with the ion remaining within the pore. Still, however, there were three windows within the channel (away from the entrances, approximately $|z| < 9$ Å) for 1 kcal/mol/Å^2 and seven for the 10 kcal/mol/Å^2 constraint where the ion was seen to leave the single-file pore, preferring the solvation environment of the penetrating water in the membrane core. Clearly, the flexibility of the protein plays a considerable role ion stabilizing the ion in this narrow pore. This would not be included in a model of permeation based on a rigid protein or continuum solvent.

Fig. 12A shows the PMF for the permeation of Cl^- through gA. Because of the complexities occurring deep within the channel, which most likely are not well averaged in the simulations, we show only the PMF for the entrance of the ion from just outside the channel to just inside the single-file column. Despite the large perturbations to protein and water penetration into the bilayer, the Cl^- ion experiences a large barrier at all positions inside the channel. This barrier extends to the channel center (not shown), in agreement with recent model calculations of Dorman and Jordan [32]. The large disruption to the protein and membrane structure when the anion moves deep into the channel is in itself clear evidence that that ion would be unfavorable deep within the channel. The steep barrier presented to the anion appears far outside the channel (even beyond $z = 14$ Å) before the backbone contributes substantially to solvation, consistent with the observation that anions do not enter into the pore region in unbiased simulation [27], and with the mechanism suggested by Sung and Jordan in 1987 [31], who proposed that the electrostatic field due to the radiating carbonyl groups in the last turn of the gA helix would create a barrier for anions. In fact, the PMF continues to climb until ~ 8 Å from the channel center for then to level off—presumably due to the deep penetration of water and the protein distortion as seen in Fig. 11C and D. To demonstrate that the flexibility of the protein backbone plays a role in the stabilization of the anions in the channel, we have repeated the umbrella sampling simula-tions with constraints on backbone atoms, as mentioned above.
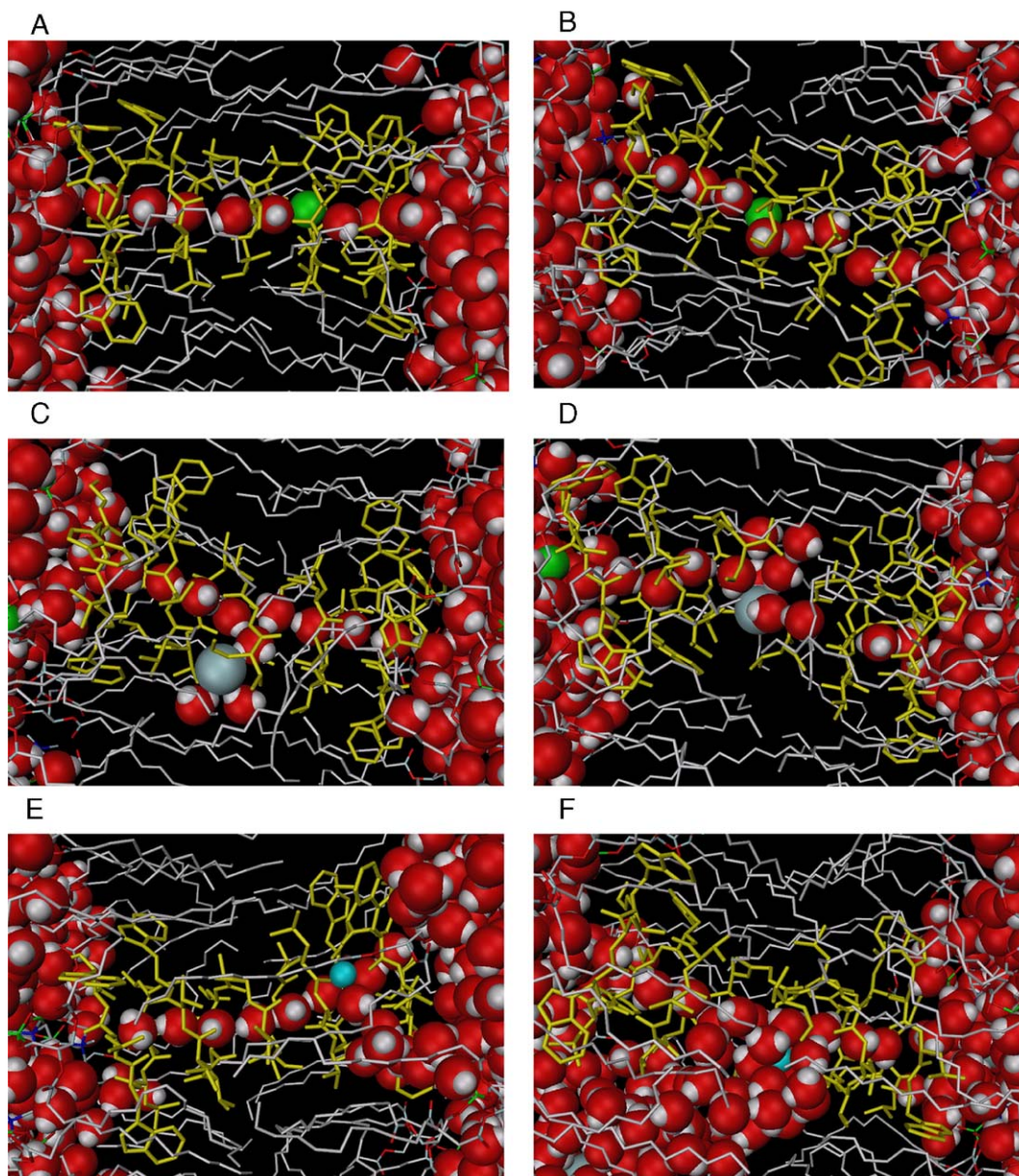
Fig. 11. (A and B) Two typical configurations when a monovalent ion, K^+ is held inside the channel; one within a monomer and one near the center of the gA channel during umbrella sampling simulation. (C and D) Showing the change in hydration environment of the protein when a Cl^- ion is held at two positions within the channel. (E and F) The situation when a Ca^{2+} is held at two positions within the channel. The same color scheme as in Fig. 2 is used with K^+, Cl^- and Ca^{2+} are green, gray and cyan, respectively.

It can be seen in Fig. 12A that, when 1 kcal/mol/Å^2 (dash-dot curve) or 10 kcal/mol/Å^2 (dotted curve) constraints are placed on the backbone atoms, the barrier rises by approximately 5 kcal/mol for the entry of a Cl^- into the single-file pore of gA.

In the case of Ca^{2+}, a large amount of water has moved from the bulk to solvate the ion, as shown in Fig. 11E and F. In E, a stream of water can be seen penetrating the membrane to reach the ion held within the channel. In F, the ion is held near the center of the channel and a large amount of water has completely disrupted the bilayer to solvate the excess charge in the middle of the hydrophobic core. Clearly, the protein alone is unable to stabilize a divalent ion in the center of the membrane. (Similar behavior has been observed in an unrelated

study investigating the stability of charged amino acids, attached to trans-membrane helices, through a membrane (T. W. Allen, manuscript in preparation).

To show that Ca^{2+} will visit the center of the channel only rarely, we turn to the equilibrium PMF. Fig. 12B shows the PMF for the entrance of Ca^{2+} into gA. Again a steep barrier is observed as the divalent cation enters the channel. In this case, there is no repulsive component outside the channel as there was for the anion, but once the narrow column approaches the entrance, the barrier rises steeply. As for the anion case, because of the large perturbations to the bilayer, the water and the protein when ion is deep inside the channel, the PMF is only shown for the entry process. Despite the large perturbations, the
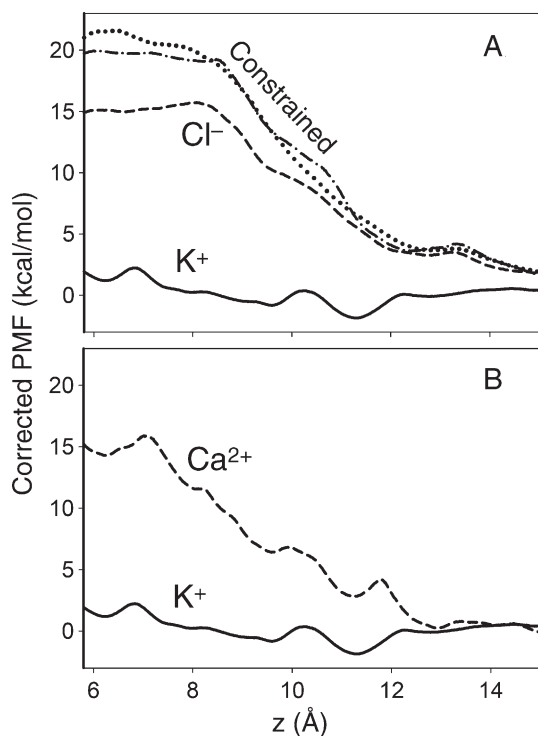
Fig. 12. (A) Corrected PMF for Cl^-. Only the entrance region is shown from ~6 to 15 Å. As a comparison, all simulations were repeated with constrained backbone (see text) shown as dash-dot (1 kcal/mol/Å^2 constraint) and dotted (10 kcal/mol/Å^2 constraint) curves to highlight the role of flexibility in selectivity. (B) The PMF for a Ca^{2+} is shown for the same entrance region. All PMFs have been matched to the K^+ PMF at $z = 20$ Å.

free energy remains high throughout the channel, including the channel center (not shown). At no point inside, the channel is the divalent cation favored over bulk electrolyte. Again, the large disruptions to protein and membrane structure themselves demonstrate that it is highly unfavorable for a divalent cation to exist deep within the channel.

For divalent ions, the artifact corrections are much larger than those for the monovalent ion, as seen in Fig. 5A and B (dashed curves). Fig. 5A shows that the periodicity correction for a divalent ion, for the small system, is −6.5 kcal/mol at the channel center, whereas the dielectric correction has a maximum value of −8.4 kcal/mol. Thus, while the total correction for a monovalent ion is approximately −4 kcal/mol near the channel center, for divalent ions, the total correction is approximately −15 kcal/mol. Thus, any attempt to estimate the free energy of a multivalent ion through a narrow ion channel without correction for simulation artifacts will result in a significant error. The PMF in Fig. 12B has been adjusted by adding these corrections, which is as large as −10 /mol at $z = 6$ Å where the plot in Fig. 12B terminates. Thus, the correction has brought the barrier at $z = 6$ Å down from approximately 25 kcal/mol to 15 kcal/mol. As discussed in the Introduction, Ca^{2+} ions bind weakly to the gA channel near $z \approx 13$ Å. A shallow minimum in free energy is observed near this point in the PMF. However, this well does not appear deep enough to explain the weak block of monovalent cation conductance seen experimentally [90]. We calculated a dissociation coefficient for the

channel of 3.2 M for Ca^{2+}, which can be compared to the experimentally derived estimate of ~1 M [37]. Though the deviation between predicted observables and experimental results is comparable to that the K^+, it is most likely that an accurate prediction of the solvation free energy of the divalent ion requires the inclusion of electronic polarizability.

3. Discussion and conclusion

In this study, we have described strategies for implementing a range of computations aimed at investigating permeation mechanisms and selectivity of narrow ion channels. Using umbrella sampling, we obtain well converged PMFs through the gA channel, which yield semi-quantitative agreement with all available experimental recordings of channel conductance and dissociation constants. We caution that this agreement is based on a simplified framework corresponding to a 1-ion Nernst–Planck diffusion pore theory. While this framework is used to compare the computational results to limiting concentration data (g_{max}), strict 1-ion permeation is valid only at low and moderate concentration in gA and double occupancy occurs at high concentration. Thus, the calculations aim only to provide rough order of magnitude estimates. Given the challenges of reproducing accurately bulk and single-file pore solvation environments without the assistance of many-body terms in the force field, the agreement must be considered an unexpectedly good outcome.

We have examined the sensitivity of our results to the choice of three popular force fields that have been used extensively in studies of ion permeation. For example, the KcsA potassium channel has been studied using CHARMM27 [23,80,91,92], AMBER94 [93,94] and GROMOS87 [95–97]) force fields. Though recent improvements in the GROMOS force field have been made (GROMOS53A [98]), we focused on the ability of the extensively employed united atom GROMOS87 force field to model ion permeation through the narrow pore of gA. Among the tested fixed-charge non-polarizable force fields, the CHARMM27 force field best reproduces gas phase ion–water, ion–NMA, bulk phase ion–NMA and gA maximum conductance and dissociation coefficients, though one must stress that the accord is far from perfect. The AMBER94 force field, which provides similar energetics in gas and liquid phase water and NMA, also yields reasonable agreement with channel conductance and binding affinities. The united atom GROMOS87 force field appears to be unable to reproduce interactions with protein, or gA observables, mostly likely because the protein backbone representation is not sufficiently polar in nature.

One reason that we were relatively successful in being able to predict experimental observables in semi-quantitative agreement with experimental results was that we corrected for some important simulation artifacts. For example, the effect of periodicity of the finite-size system was estimated by either continuum electrostatics or by recalculating the PMF with a much larger membrane — in both cases providing a ~2 kcal/mol stabilization. In addition, the lack of induced polarization in the lipid hydrocarbon was estimated using continuum electrostatics and with a model of polarizability based on classical

Drude oscillators, yielding in both case a reduction of the central barrier in the PMF by 2–3 kcal/mol. When both of these corrections are included, the resulting PMF is found to provide reasonable agreement with experimental binding and conductance in the case of K^+. The corrections for simulation artifacts are rather large (about 15 kcal/mol) in the case of the divalent Ca^{2+}, but still much less than the overall barrier, which remains high as expected for an impermeable ion.

Because a 1D PMF cannot describe the free energy of an ion in the channel relative to bulk electrolyte (integrations over lateral displacements diverging outside the pore), we created a 2D free energy surface to describe ion conduction. This was done in both a fixed membrane-normal frame (relevant to conduction) and an instantaneous channel axis frame (relevant to ion–protein interactions during translocation across the membrane). We determined that the ion binds predominantly to an "outer" binding site, near $z = 11.3$ Å from the channel center, which is an off-axis binding site where the ion is hydrated by 3 water molecules on average. It also binds to a lesser extent to an inner binding site near $z = 9.7$ Å, which is on-axis and hydrated by just 2 water molecules deep in the single-file pore. The off-axis binding and subsequent greater translational freedom may pose a challenge to experiments, which base ion binding positions on changes in backbone chemical shifts.

Intuitively, one imagines that an ion entering a narrow pore, in a process where 5 of its ~ 7 water molecules are being stripped away, will experience a very large dehydration barrier. That is not the case because the single-file water does an amazing job of stabilizing the ion-providing approximately half of the ion's bulk hydration free energy though there are only two nearest neighbor water molecules. The importance of the water in ion permeation through gA led us to examine the role of electronic polarizability of the strongly aligned water. TIP3P does a good job of modeling single-file water – with electronic polarizability accounting for only a fraction of a kcal/mol – as shown with Drude oscillator-based water model. We also examined more closely the role of hydration in the permeation process — in particular, the dehydration process upon entry and the flipping of the single-file water that is essential for ion translocation. We have found that dehydration is a continuous process as a function of ion position that is adequately sampled in these simulations. However, the water column flipping is a slow process, with a barrier of 2–3 kcal/mol. The barrier presented to an ion approaching the channel is very different depending on the orientation of the water column, and one must adequately sample the entire distribution of water chain alignment sin order to model permeation with a single-ion positional coordinate. Furthermore, this water chain can account for a structure-based coupling of ions across the channel and we have calculated the contribution of the coupling of the dipole to the external membrane potential, as a function of ion position, to the potential of mean force governing conduction.

We have shown that it is possible to construct PMFs that allow for mechanistic insight into ion permeation selectivity in the gA channel. Both Cl^- and Ca^{2+} face steep barriers, excluding the ions from the channel. In the case of Cl^-, the barrier extended well outside the channel, presumably owing to the negative electric field arising from the outer helix turn carbonyl dipoles. For the divalent ion Ca^{2+}, the barrier became steep only as the ion entered the pore. Experimentally observed weak blocking of monovalent current by divalent ions corresponds to a free energy well that is approximately in the correct location ($z = 13$ Å) but which is too shallow. Though the K_D for Ca^{2+} was predicted with semi-quantitative accuracy, it is likely that induced electronic polarizability will be needed to accurately model the interactions between divalent ions, protein and water. During the simulations with Cl^- and Ca^{2+}, we observed drastic changes to the hydration environment of the ions held deep within the channel and, in some cases, large changes to the protein structure. The protein cannot effectively solvate either of these ions and, as a result, bulk water penetrates the hydrophobic core of the membrane in an effort to stabilize the ions. This clearly demonstrates that gA is highly selective for monovalent cations over divalent cations and anions, and that the protein charge distribution appears specifically well tuned to the permeation of monovalent cations.

Though we wish to stress the limitations in the current methods, the semi-quantitative prediction of experimental observables make us conclude that careful application of the MD-PMF approach with modern all-atom force fields represents a promising avenue for understanding the function of ion channels.

Acknowledgments

References

[1] A. Hodgkin, B. Katz, The effect of sodium ions on the electrical activity of the giant axon of the squid, J. Physiol. (Lond.) 108 (1949) 37–77.

[2] A. Hodgkin, A. Huxley, A quantitative description of membrane current and its application to conduction and excitation of nerve, J. Physiol. (Lond.) 117 (1952) 500–544.

[3] D. Doyle, J. Cabral, R. Pfuetzner, A. Kuo, J. Gulbis, S. Cohen, B. Chait, R. MacKinnon, The structure of the potassium channel: molecular basis of K^+ conduction and selectivity, Science 280 (1998) 69–77.

[4] Y. Jiang, A. Lee, J. Chen, M. Cadene, B. Chait, R. MacKinnon, The open pore conformation of potassium channels, Nature 417 (2002) 523–526.

[5] Y. Jiang, A. Lee, J. Chen, V. Ruta, M. Cadene, B.T.C. et al, X-ray structure of a voltage-dependent K+ channel, Nature 423 (2003) 33–41.

[6] A. Miyazawa, Y. Fujiyoshi, N. Unwin, Structure and gating mechanism of the acetylcholine receptor pore, Nature 423 (2003) 949–955.

[7] G. Chang, R. Spencer, A. Lee, M. Barclay, D. Rees, Structure of the mscl homolog from mycobacterium tuberculosis: a gated mechanosensitive ion channel, Science 282 (1998) 2220–2226.

[8] R. Dutzler, E.B. Campbell, M. Cadene, B.T. Chait, R. MacKinnon, X-ray structure of a clc chloride channel at 3.0 a reveals the molecular basis of an ion selectivity, Nature 415 (2002) 287–294.

[9] M. Karplus, G. Petsko, Molecular dynamics simulations in biology, Nature 347 (1990) 631–639.

[10] D.W. Urry, The gramicidin A transmembrane channel: a proposed π_{LD} helix, Proc. Natl. Acad. Sci. U. S. A. 68 (1971) 672–676.

[11] A.S. Arseniev, A.L. Lomize, I.L. Barsukov, V.F. Bystrov, Gramicidin A trans-membrane ion-channel three-dimensional structure reconstruction based on NMR spectroscopy and energy refinement (in Russian), Biol. Membr. 3 (1986) 1077–1104.

[12] L.E. Townsley, W.A. Tucker, S. Sham, J.F. Hinton, Structures of gramicidins A, B, and C incorporated into sodium dodecyl sulfate micelles, Biochemistry 40 (2001) 11676–11686.

[13] R.R. Ketchem, B. Roux, T.A. Cross, High resolution refinement of a solid-state NMR-derived structure of gramicidin A in a lipid bilayer environment, Structure 5 (1997) 1655–11669.

[14] T.W. Allen, O.S. Andersen, B. Roux, The structure of gramicidin A in a lipid bilayer environment determined using molecular dynamics simulations and solid-state NMR data, J. Am. Chem. Soc. 125 (2003) 9868–9877.

[15] S.B. Hladky, B. Urban, D. Haydon, Ion movements in pores formed by gramicidin A, Membr. Transp. Processes 3 (1979) 89–103.

[16] G. Eisenman, R. Horn, Ionic selectivity revisited: the role of kinetic and equilibrium processes in ion permeation through channels, J. Membr. Biol. 76 (1983) 197–225.

[17] O. Andersen, R. Koeppe, Molecular determinants of channel function, Physiol. Rev. 72 (1992) S89–S158.

[18] D. Busath, The use of physical methods in determining gramicidin channel structure and function, Ann. Rev. Physiol. 55 (1993) 473–501.

[19] O.S. Andersen, R.E. Koeppe II, B. Roux, Gramicidin channels, IEEE Trans. Nanobio-Sci. 4 (2005) 10–20.

[20] T.W. Allen, O.S. Andersen, B. Roux, On the importance of flexibility in studies of ion permeation, J. Gen. Physiol. 124 (2004) 679–690.

[21] B. Roux, Computational studies of the gramicidin channel, Acc. Chem. Res. 35 (2002) 366–375.

[22] J.D. Faraldo-Gomez, L.R. Forrest, M. Baaden, P.J. Bond, C. Domene, G. Patargias, J. Cuthbertson, M.S.P. Sansom, Conformational sampling and dynamics of membrane proteins from 10-nanosecond computer simulations, Proteins 57 (2004) 783–791.

[23] B. Roux, M. Karplus, Ion transport in the gramicidin channel: free energy of the solvated right-handed dimer in a model membrane, J. Am. Chem. Soc. 115 (1993) 3250–3262.

[24] T.W. Allen, T. Bastug, S. Kuyucak, S.H. Chung, Gramicidin A channel as a test ground for molecular dynamics force fields, Biophys. J. 84 (2003) 2159.

[25] T. Bastug, S. Kuyucak, Test of molecular dynamics force fields in gramicidin A, Ero. Biophys. J. 34 (2005) 377–382.

[26] T.W. Allen, O.S. Andersen, B. Roux, Energetics of ion conduction through the gramicidin channel, PNAS 101 (2004) 117–122.

[27] T.W. Allen, O.S. Andersen, B. Roux, Ion permeation through a narrow channel: using gramicidin to ascertain all-atom molecular dynamics potential of mean force methodology and biomolecular force fields, Biophys. J. 90 (2006) 3447–3468.

[28] V.B. Myers, D.A. Haydon, Ion transfer across lipid membranes in the presence of gramicidin A, Biochim. Biophys. Acta 274 (1972) 313–322.

[29] B. Conway, On the free energy of ionic hydration, J. Solution Chem. 7 (1978) 721.

[30] U.D. W., C.M. Venkatachalam, K.U. Prasad, R.J. Bradley, G. Parenti-Castelli, G. Lenaz, Conduction process of the gramicidin channel, Int. J. Quantum Chem., Quantum Biol. Symp. 8 (1981) 385–399.

[31] S. Sung, P.C. Jordan, Why is gramicidin valence selective? A theoretical study, Biophys. J. 51 (1987) 661–672.

[32] V.L. Dorman, P.C. Jordan, Ionic permeation free energy in gramicidin: a semi-microscopic perspective, Biophys. J. 86 (2004) 3529–3541.

[33] B. Roux, Valence selectivity of the gramicidin channel: a molecular dynamics free energy perturbation study, Biophys. J. 71 (1996) 3177–3185.

[34] B.G. Cox, G.R. Hedwig, A.J. Parker, D.W. Watts, Solvation of ions: XIX. Thermodynamic properties for transfer of single ions between protic and dipolar aprotic solvents, Aust. J. Chem. 27 (1974) 477–501.

[35] S. Edwards, B. Corry, S. Kuyucak, S.-H. Chung, Continuum electrostatics fails to describe ion permeation in the gramicidin channel, Biophys. J. 83 (2002) 1348–1360.

[36] G.A. Olah, H.W. Huang, W. Liu, Y. Wu, Location of ion-binding sites in the gramicidin channel by X-ray diffraction, J. Mol. Biol. 218 (1991) 847.

[37] D.W. Urry, T.L. Trapane, J.T. Walker, K.U. Prasad, On the relative lipid membrane permeability of Na+ and Ca2+. A physical basis for the messenger role of Ca2+, J. Biol. Chem. 257 (1982) 6659–6661.

[38] A. Golovanov, I. Barsukov, A. Arseniev, V. Bystrov, S. Sukhanov, L. Barsukov, The divalent cation-binding sites of gramicidin A transmembrane ion-channel, Biopolymers 31 (1991) 425–434.

[39] F. Tian, T. Cross, Cation transport: an example of structural based selectivity, J. Mol. Biol. 285 (1999) 1993–2003.

[40] A.T. Blades, P. Jayaweera, M.G. Ikonomou, P. Kebarle, Studies of alkaline earth and transition metal m++ gas phase ion chemistry, J. Chem. Phys. 92 (1990) 5900–5906.

[41] J.M. Lehn, J.P. Savage, [2]-crypates: stability and selectivity of alkali and alkaline-earth macrobicyclic complexes, J. Am. Chem. Soc. 97 (1975) 6700–6707.

[42] T. Woolf, B. Roux, Structure, energetics and dynamics of lipid–protein interactions: a molecular dynamics study of the gramicidin A channel in a dmpc bilayer, Prot. Struct. Funct. Gen. 24 (1996) 92–114.

[43] B.R. Brooks, R.E. Bruccoleri, B.D. Olafson, D.J. States, S. Swaminathan, M. Karplus, CHARMM: a program for macromolecular energy minimization and dynamics calculations, J. Comput. Chem. 4 (1983) 187–217.

[44] A.D. MacKerell Jr., D. Bashford, M. Bellot, R.L. Dunbrack, J.D. Evanseck, M.J. Field, S. Fischer, J. Gao, H. Guo, S. Ha, D. Joseph-McCarthy, L. Kuchnir, K. Kuczera, F.T.K. Lau, C. Mattos, S. Michnick, T. Ngo, D.T. Nguyen, B. Prodhom, W.E. Reiher III, B. Roux, B. Schlenkrich, J. Smith, R. Stote, J. Straub, M. Watanabe, J. Wiorkiewicz-Kuczera, M. Karplus, All-atom empirical potential for molecular modeling and dynamics studies of proteins, J. Phys. Chem., B 102 (1998) 3586–3616.

[45] M. Schlenkrich, J. Brickmann, A.J. MacKerell, M. Karplus, An empirical potential energy function for phospholipids: criteria for parameters optimization and applications, in: K. Merz, B. Roux (Eds.), Biol. Membr.. A Molecular Perspective from Computation and Experiment, Birkhauser, Boston, 1996, pp. 31–81.

[46] W.L. Jorgensen, J. Chandrasekhar, J.D. Madura, R.W. Impey, M.L. Klein, Comparison of simple potential functions for simulating liquid water, J. Chem. Phys. 79 (1983) 926–935.

[47] D. Beglov, B. Roux, Finite representation of an infinite bulk system: solvent boundary potential for computer simulations, J. Chem. Phys. 100 (1994) 9050–9063.

[48] W. Cornell, P. Cieplak, C. Bayly, I. Gould, K.M. Merz Jr., D. Ferguson, D. Spellmeyer, T. Fox, J. Caldwell, P. Kollman, A second generation force field for the simulation of proteins and nucleic acids, J. Am. Chem. Soc. 117 (1995) 5179–5197.

[49] W. van Gunsteren, X. Daura, A. Mark, GROMOS force field, in: P. von Ragu Schelyer (Ed.), Encyclopaedia of Computational Chemistry, e.-i.-c, vol. 2, John Wiley and Sons, Ltd., 1999, pp. 1211–1216.

[50] J. Åqvist, Ion water interaction potential derived from free energy perturbation simulations, J. Phys. Chem. 94 (1990) 8021–8024.

[51] H. Berendsen, J. Postma, W. van Gunsteren, J. Hermans, Interaction models for water in relation to proteins hydration, in: B. Pullman (Ed.), In Intermolecular Forces, Reidel, Dordrecht, 1981, pp. 331–342.

[52] T. Straatsma, H. Berendsen, J. Postma, Free energy of ionic hydration: analysis of a thermodynamic integration technique to evaluate free energy differences by molecular dynamics simulations, J. Chem. Phys. 89 (1988) 5876–5886.

[53] T. Darden, D. York, L. Pedersen, Particle mesh Ewald: a n log(n) method for Ewald sums in large systems, J. Chem. Phys. 98 (1993) 10089–10092.

[54] J.P. Ryckaert, G. Ciccotti, H.J.C. Berendsen, Numerical integration of the cartesian equation of motions of a system with constraints: molecular dynamics of *n*-alkanes, J. Comp. Chem. 23 (1977) 327–341.

[55] S.E. Feller, Y.H. Zhang, R.W. Pastor, B.R. Brooks, Constant pressure molecular dynamics simulation—the Langevin piston method, J. Chem. Phys. 103 (1995) 4613–4621.

[56] B. Roux, M. Karplus, Ion transport in a gramicidin-like channel: structure and thermodynamics, Biophys. J. 59 (1991) 961–981.

[57] B. Roux, Statistical mechanical equilibrium theory of selective ion channels, Biophys. J. 77 (1999) 139–153.

[58] G.M. Torrie, J.P. Valleau, Nonphysical sampling distributions in Monte Carlo free-energy estimation: umbrella sampling, J. Comp. Physiol. 23 (1977) 187–199.

[59] S. Kumar, D. Bouzida, R.H. Swendsen, P.A. Kollman, J.M. Rosenberg, The weighted histogram analysis method for free-energy calculations on biomolecules. I. The method, J. Comp. Chem. 13 (1992) 1011–1021.

[60] H.A. Stern, S.E. Feller, Calculation of the dielectric permittivity profile for a nonuniform system: application to a lipid bilayer simulation, J. Chem. Phys. 118 (2003) 3401–3412.

[61] D.R. Lide (Ed.), CRC Handbook of Chemistry and Physics, 72nd Edition (1991–1992), CRC Press Inc., Boston, 1992.

[62] P.H. Hunenberger, J.A. McCammon, Ewald artifacts in computer simulations of ionic solvation and ion–ion interaction: a continuum electrostatics study, J. Chem. Phys. 110 (1999) 1856–1872.

[63] P.C. Jordan, R.J. Bacquet, J.A. McCammon, P. Tran, How electrolyte shielding influences the electrical potential in transmembrane ion channels, Biophys. J. 55 (1989) 1041–1052.

[64] G. Lamoureux, A.D. MacKerell, B. Roux, A simple water model with Drude oscillator polarizability, J. Chem. Phys. 119 (2003) 5185–5197.

[65] J. Åqvist, A. Warshel, Energetics of ion permeation through membrane channels. solvation of Na^+ by gramicidin A, Biophys. J. 56 (1989) 171–182.

[66] D. Levitt, Interpretation of biological channel flux data—reaction-rate theory versus continuum theory, Ann. Rev. Biophys. Chemist. 15 (1986) 29–57.

[67] B. Roux, M. Karplus, Ion transport in a gramicidin-like channel: dynamics and mobility, J. Phys. Chem. 95 (1991) 4856–4868.

[68] B. Roux, B. Prod'hom, M. Karplus, Ion transport in the gramicidin channel: molecular dynamics study of single and double occupancy, Biophys. J. 68 (1995) 876–892.

[69] B.J. Berne, M. Borkovec, J.E. Straub, Classical and modern methods in reaction rate theory, J. Phys. Chem. 92 (1988) 3711–3725.

[70] S. Crouzy, T. Woolf, B. Roux, A molecular dynamics study of gating in dioxolane-linked gramicidin A channels, Biophys. J. 67 (1994) 1370–1386.

[71] D.D. Busath, C.D. Thulin, R.W. Hendershot, L.R. Phillips, P. Maughan, C.D. Cole, N.C. Bingham, S. Morrison, L.C. Baird, R.J. Hendershot, M. Cotten, T.A. Cross, Noncontact dipole..., Biophys. J. 75 (2003) 2830–2844.

[73] N. Jing, K.U. Prasad, D.W. Urry, The determination of binding constants of micellar-packaged gramicidin A by 13C- and 23Na-NMR, Biochim. Biophys. Acta 1238 (1995) 1–11.

[74] J.F. Hinton, W.L. Whaley, D.C. Shungu, R.E. Koeppe II, F.S. Millett, Equilibrium binding constant for the group I metal cations with gramicidin—a determined by competition studies and Tl^+-205 nuclear magnetic resonance spectroscopy, Biophys. J. 50 (1986) 539–544.

[75] N. Thompson, G. Thompson, C.D. Cole, M. Cotten, T.A. Cross, D.D. Busath, Noncontact dipole effects on channel permeation: IV. Kinetic model of 5F-Trp13 gramicidin A currents, Biophys. J. 81 (2001) 1245–1254.

[76] G. Lamoureux, B. Roux, Absolute hydration free energy scale for alkali and halide ions established from simulations with a polarizable force field. J. Am. Chem. Soc. (in press).

[77] G. Hummer, S. Garde, A. Garcia, A. Pohorille, L. Pratt, An information theory model of hydrophobic interactions, Proc. Natl. Acad. Sci. U. S. A. 93 (1996) 8951–8955.

[78] B. Roux, S. Berneche, On the potential functions used in molecular dynamics simulations of ion channels, Biophys. J. 82 (2002) 1681–1684.

[79] B. Roux, Nonadditivity in cation-peptide interactions: a molecular dynamics and ab initio study of Na^+ in the gramicidin channel, Chem. Phys. Lett. 212 (1993) 231–240.

[80] S. Bernèche, B. Roux, Energetics of ion conduction through the K+ channel, Nature 414 (2001) 73–77.

[81] A. Finkelstein, O.S. Andersen, The gramicidin A channel: a review of its permeability characteristics with special reference to the single-file aspect of transport, J. Membr. Biol. 59 (1981) 155–171.

[82] D.H.J. Mackay, P.H. Berens, K.R. Wilson, A.T. Hagler, Structure and dynamics of ion transport through gramicidin A, Biophys. J. 46 (1984) 229–248.

[83] A. Parsegian, Energy of an ion crossing a low dielectric membrane: solution to four relevant electrostatic problems, Nature 221 (1969) 844–846.

[84] D. Levitt, Electrostatic calculations for an ion channel: I. Energy and potential profiles and interactions between ions, Biophys. J. 22 (1978) 209–219.

[85] B. Roux, S. Bernèche, W. Im, Ion channels, permeation and electrostatics: insight into the function of KcsA, Biochem. 39 (2000) 13295–13306.

[86] P.G. Bolhuis, C. Dellago, D. Chandler, Reaction coordinates of biomolecular isomerization, Proc. Natl. Acad. Sci. U. S. A. 97 (2000) 5877–5882.

[87] W. Im, B. Roux, Ions and counterions in a biological channel: a molecular dynamics simulation of ompf porin from *Escherichia coli* in an explicit membrane with 1 m KCl aqueous salt solution, J. Mol. Biol. 391 (2002) 1177–1197.

[88] R. Pomès, B. Roux, Molecular mechanism of H+ conduction in the single-file water chain of the gramicidin channel, Biophys. J. 82 (2002) 2304–2316.

[90] E. Bamberg, P. Lauger, Blocking the gramicidin channel by divalent ions, J. Membr. Biol. 35 (1977) 351–375.

[91] T.W. Allen, S. Kuyucak, S.H. Chung, Molecular dynamics study of the KcsA potassium channel, Biophys. J. 77 (1999) 2502–2516.

[92] T. Allen, A. Bliznyuk, A. Rendell, S. Kuyucak, S. Chung, The potassium channel: structure, selectivity and diffusion, J. Chem. Phys. 112 (2000) 8191–8204.

[93] L. Guidoni, V. Torre, P. Carloni, Potassium and sodium binding to the outer mouth of the K^+ channel, Biochemistry 38 (1999) 8599–8604.

[94] L. Guidoni, V. Torre, P. Carloni, Water and potassium dynamics inside the KcsA K(+) channel, FEBS Lett. 477 (2000) 37–42.

[95] I. Shrivastava, M. Sansom, Simulations of ion permeation through a potassium channel: molecular dynamics of KcsA in a phospholipid bilayer, Biophys. J. 78 (2000) 557–570.

[96] P. Biggin, G. Smith, I. Shrivastava, S. Choe, M. Sansom, Potassium and sodium ions in a potassium channel studied by molecular dynamics simulations, Biochim. Biophys. Acta 1510 (2001) 1–9.

[97] J. Åqvist, V. Luzhkov, Ion permeation mechanism of the potassium channel, Nature 404 (2000) 881–884.

[98] C. Oostenbrink, A. Villa, A.E. Mark, W.F. van Gunsteren, A biomolecular force field based on the free enthalpy of hydration and solvation: the GROMOS force-field parameter sets 53a5 and 53a6, J. Comput. Chem. 25 (2004) 1656–1676.

[99] B. Roux, S. Bernèche, On the potential functions used in molecular dynamics simulations of ion channels, Biophys. J. 82 (2002) 1681–1684.

[100] R.M. Noyes, Thermodynamics of ion hydration as a measure of effective dielectric properties of water, J. Am. Chem. Soc. 84 (1962) 513–522.

[101] I.V. Vorobyov, V.M. Anisimov, A.D. MacKerell Jr., Polarizable empirical force field for alkanes based on the classical drude oscillator model, J. Phys. Chem. B. 109 (2005) 18988–18999.